Journal of
Materials Chemistry C

Accepted Manuscript

This article can be cited before page numbers have been issued, to do this please use: L. Wang, H. Huang, Y. Wang, S. Zhuang, B. Pan, X. Yang, C. Yang and B. Wang, *J. Mater. Chem. C*, 2013, DOI: 10.1039/C3TC30832D.

This is an *Accepted Manuscript*, which has been through the RSC Publishing peer review process and has been accepted for publication.

Accepted Manuscripts are published online shortly after acceptance, which is prior to technical editing, formatting and proof reading. This free service from RSC Publishing allows authors to make their results available to the community, in citable form, before publication of the edited article. This *Accepted Manuscript* will be replaced by the edited and formatted *Advance Article* as soon as this is available.

To cite this manuscript please use its permanent Digital Object Identifier (DOI®), which is identical for all formats of publication.

More information about *Accepted Manuscripts* can be found in the **Information for Authors**.

Please note that technical editing may introduce minor changes to the text and/or graphics contained in the manuscript submitted by the author(s) which may alter content, and that the standard **Terms & Conditions** and the **ethical guidelines** that apply to the journal are still applicable. In no event shall the RSC be held responsible for any errors or omissions in these *Accepted Manuscript* manuscripts or any consequences arising from the use of any information contained in them.

View Article Online
DOI: 10.1039/C3TC30832D

Controllably Tunable Phenanthroimidazole/Carbazole Hybrid Bipolar Host Materials for Efficient Green Electrophosphorescent Devices

Hong Huang,[a] Yixing Wang,[a] Bo Wang,[a] Shaoqing Zhuang,[a] Biao Pan,[a] Xiao Yang,[a] Lei Wang,*[a] Chuluo Yang.*[ab]

[a]*Wuhan National Laboratory for Optoelectronics, Huazhong University of Science and Technology, Wuhan 430074, P. R. China.*
[b]*Department of Chemistry, Wuhan University, Wuhan 430072, P. R. China*
Email：wanglei@mail.hust.edu.cn; clyang@whu.edu.cn.

A series of phenanthroimidazole/carbazole (1 : 2) hybrids as bipolar host materials have been designed and synthesized through facile typical Ullmann reactions. These compounds with regid configurations exhibit excellent thermal and morphological stability with high glass transition temperatures (T_g) (143 ~ 282 ℃). Their photoelectronic properties, energy levels, charge transport mobility, film morphologies can be controllably tuned through judicious engineering of the linkage modes between the two carbazole groups and the 2,5-diphenyl-1,3,4-phenanthroimidazole (*para* and *meta*).. The promising physical properties of these new compounds made them suitable for use as hosts doped with Ir-based phosphor for realizing highly efficient phosphorescent organic light emitting diodes (PhOLEDs). Green device hosted by compound PhBIDmpCP shows a maximum current efficiency of 74.3 cd/A, and a maximum power efficiency of 74.4 lm/W (corresponding EQE_{max} = 20.2%).

1. Introduction

Organic light-emitting diodes (OLEDs) have attracted much interest due to their potential applications in organic flat-panel displays and flexible lighting sources[1]. And phosphorescent emitters have been recognized as the most effective approach to achieve high efficiency devices since both the singlet and triplet excitons can be harvested in this way[2-5]. Generally, phosphorescent organic light-emitting diodes (PhOLEDs) adopt a host-guest system to reduce concentration quenching and T_1-T_1

View Article Online
DOI: 10.1039/C3TC30832D

annihilation[6]. As a result, a diverse of host materials have been developed based on carbozole and their derivatives.. However, those host materials such as *N,N′*-dicarbazolyl-3,5-benzene (mCP)[7], 4,4'-di(9H-carbazol-9-yl)-1,1'-biphenyl (CBP)[8] and tris(4-(9H-carbazol-9-yl)phenyl) amine (TCTA)[9] with hole-transporting properties, show an unbalanced carrier-transporting property, which is harmful to the stability and the efficiency of PhOLEDs. With the aim to solve the problem, some bipolar host materials[10-13], such as bis-4-(*N*- carbazolyl)phenyl)phenylphosphine oxide (BCPO)[14], 4,7-dicarbazol-9-yl-[1,10] phenanthroline (BUPH1)[15], and 2,5-bis(2-(9H-carbazol-9-yl)phenyl)-1,3,4-oxadiazole (*o*-CzOXD)[16], have been developed. When applying BCPO, BUPH1 and *o*-CzOXD as host material for green PhOLEDs, the maximum power efficiencies of 87.5 lm/W, 33.0 lm/W and 59.3 lm/W were achieved ,respectively.[14-16]. As indicated by literatures, an excellent host material must possess: (i) a suitable E_T for phosphors, transferring energy to the guest effectively, (ii) bipolar carrier transporting property, rendering a broad exciton-formation zone and consequently reducing the efficiency roll-off, (iii) the appropriate HOMO/LUMO levels, well matching with that of the neighboring layers, and allowing the effective charge injection and charge confinement, (iv) high thermal and morphological stability, which is required for a long operational lifetime. As mentioned before, carbazole and its derivatives have been widely used in designing host materials due to their sufficiently high triplet energy levels and good hole-transporting properties[17]. On the other hand, the phenanthroimidazole moiety has been demonstrated to be effective for the electron injection and hole blocking[18], accompanying with strong blue fluorescence[19-21]. In addition, the rigid structure of phenanthroimidazole made its derivatives possess high thermal stability. Herein, the combination of carbazole and phenanthroimidazole moieties provides a reasonable strategy for designing bipolar host materials in PhOLEDs.

In our previous work,[22] we have also developed a series of phenanthroimidazole/carbazole hybrids (1:1) as bipolar host materials, which exhibit a maximum current efficiencies ranging from 60.2 ~ 77.6 cd•A^{-1} and 49.6 ~ 57.3 cd•A^{-1} for green and yellow PhOLEDs, respectively. It was found that the hosts based

View Article Online
DOI: 10.1039/C3TC30832D

on carbazole/phenanthroimidazole hybrid conjugated through the *N*-phenyl exhibit better EL performances than those of *C2*-phenyl conjugated analogues under virtually identical conditions. However, the glass transition temperatures (T_g) of those hybrids conjugated by *N*-phenyl (pPhBINCP and mPhBINCP) is only around 110 ℃. The primary results motivate us to develop new host materials with high glass transition temperatures and balanced charge transport properties for high efficiency PhOLEDs.

In this contribution, aiming to achieve high glass transition temperatures and balance charge transport host materials for PHOLEDs, we designed and synthesized a series of bipolar host materials by the conjugation of two carbazole units to one phenanthroimidazole moiety through different linkage modes. As expected, these new compounds exhibit high thermal stabilities, with the decomposition temperatures (T_d, 5 wt % weight loss) and the glass transition temperatures (T_g) in the range of 468 ~ 514 ℃ and 143 ~ 282 ℃, respectively. The device doping the phosphorescent emitter $Ir(ppy)_3$ into the PhBIDmpCP shows a low onset voltage of 2.8 V, high brightness of 42160 cd/m^2 at 10.0 V, corresponding to a maximum current efficiency of 74.3 cd/A and a maximum power efficiency of 74.4 lm/W, as well as maximum external quantum efficieny (EQE_{max}) of 20.2%.

2. Experimental Section

2.1. General Information

All the reagents and solvents used for the synthesis were purchased from Aldrich and used without further purification. All reactions were performed under a dry nitrogen atmosphere. ^{1}H NMR and ^{13}C NMR spectra were measured on a Bruker-AF301 AT 400MHz spectrometer. Elemental analyses of carbon, hydrogen, and nitrogen were performed on an Elementar (Vario Micro cube) analyzer. Mass spectra were carried out on an Agilent (1100 LC/MSD Trap) using ACPI ionization. UV-Vis absorption spectra were recorded on a Shimadzu UV-VIS-NIR Spectrophotometer (UV-3600). PL spectra were recorded on Edinburgh instruments (FLSP920 spectrometers). Differential scanning calorimetry (DSC) was performed on

View Article Online
DOI: 10.1039/C3TC30832D

a PE Instruments DSC 2920 unit at a heating rate of 10 ℃/min from 30 to 300 ℃ under nitrogen. The glass transition temperature (T_g) was determined from the second heating scan. Thermogravimetric analysis (TGA) was undertaken with a PerkinElmer Instruments (Pyris1 TGA). The thermal stability of the samples under a nitrogen atmosphere was determined by measuring their weight loss when heating at a rate of 10 ℃/min from 30 to 700 ℃. Cyclic voltammetry (CV) measurements were carried out in a conventional three electrode cell using a glassy carbon working electrode of 2 mm in diameter, a platinum wire counter electrode, and an $Ag/AgNO_3$ (0.1 M) reference electrode on a computer-controlled EG&G Potentiostat/Galvanostat model 283 at room temperature. Reductions of all compounds were performed in dichloromethane containing 0.1 M tetrabutylammoniumhexafluorophosphate (Bu_4NPF_6) as the supporting electrolyte. And all solutions were purged with a nitrogen stream for 10 min before measurement. In the time-of-flight (TOF) transient-photocurrent technique, those samples were illuminated at 355 nm through the ITO electrode from an UV-FQ q-switched DPSS laser (pulse: 4 ns). The transient currents were measured using a digital phosphor oscilloscope (DPO 3034; bandwidth:300MHz).

2.2. Computational Details

The theoretical investigation of geometrical and electronic properties was performed with the Amsterdam Density Functional (ADF) 2009.01 program package. And the calculation was optimized by means of the B3LYP (Becke three parameters hybrid functional with Lee-Yang- Perdew correlation functionals)[23] with the 6-31G(d) atomic basis set. Then the electronic structures were calculated at τ-HCTHhyb/6–311++G(d,p)level[24]. Molecular orbital was visualized using ADFview.

2.3. Device Fabrication and Measurement

The hole-injection material MoO_3, hole-transporting material 1,4-bis[(1-naphthyl-phenyl)amino]biphenyl (NPB), electron/exciton-blocking material TCTA, and electron-transporting material 3,3'-(5'-(3-(pyridine-3-yl)phenyl)-[1,1':3',1"-terphenyl] -3,3"-diyl)dipyridine (TmPyPB) were commercially available. Commercial ITO

View Article Online
DOI: 10.1039/C3TC30832D

(indium tin oxide) coated glass with sheet resistance of 20 Ω per square was used as the substrates. Before device fabrication, the ITO glass substrates were pre-cleaned carefully and treated by oxygen plasma for 2 min. MoO_3 was firstly deposited to ITO substrate, followed by NPB, TCTA, emissive layer, and TmPyPB. Finally, a cathode composed of lithium fluoride (LiF) and aluminum (Al) was sequentially deposited onto the substrate in the vacuum of 10^{-6} Torr. The *J-V-L* of the devices was measured with a Keithley 2400 source meter equipped with a calibrated silicon photodiode. The EL spectra were measured by PR655 spectrometer. The EQE values were calculated according to previously reported methods[25].

2.4. Synthesis

The phenanthroimidazole bromide intermediates were synthesized according to the reported[20] procedure. A mixture of phenanthrenequinone (3.0 mmol), bromoaniline (15.0 mmol), bromide aromatic aldehyde (3.0 mmol) ammonium acetate (12.0 mmol) and acetic acid (200 ml) was refluxed for about 18 h under nitrogen atmosphere[26]. Then the mixture was cooled to room temperature, and the solid product was collected after filtration and washing with water and CH_3OH. The product was dried under vacuum and used directly for the next step.

1,2-bis(4-bromophenyl)-1H-phenanthro[9,10-d]imidazole (1). Yield: 78%. ^{1}H NMR ($CDCl_3$, 400 MHz) δ (ppm): 8.86 ~ 8.84 (d, *J* = 8.0 Hz, 1H)， 8.79 ~ 8.77 (d, *J* = 8.4 Hz, 1H), 8.71 ~ 8.69 (d, *J* = 8.0 Hz, 1H), 7.96 ~ 7.94 (d, *J* = 7.6 Hz, 2H), 7.75 ~ 7.67 (m, 2H), 7.57 ~ 7.53 (m, 1H), 7.48 ~ 7.41 (m, 4H), 7.35 ~ 7.26 (m, 1H), 7.26 ~ 7.20 (m, 3H). ^{13}C NMR (100 MHz, $CDCl_3$) δ (ppm): 149.68, 139.60, 138.09, 131.67, 130.92, 130.75, 129.48, 128.39, 127.94, 127.52, 126.55, 126.02, 125.34, 124.28, 123.15, 122.84, 122.60, 120.70. MS (APCI): calcd for $C_{27}H_{16}Br_2N_2$: 526.0, found, 527.0 $(M+H)^+$.

1-(3-bromophenyl)-2-(4-bromophenyl)-1H-phenanthro[9,10-d]imidazole (2). Yield: 80%. ^{1}H NMR ($CDCl_3$, 400 MHz) δ (ppm): 8.84 ~ 8.82 (d, *J* = 7.6 Hz, 1H), 8.79 ~ 8.77 (d, *J* = 8.0 Hz, 1H), 8.71 ~ 8.69 (d, *J* = 8.4 Hz, 1H), 7.81 ~ 7.73 (m, 2H), 7.69 ~ 7.65 (m, 2H), 7.56 ~ 7.43 (m, 7H), 7.34 ~ 7.30 (m, 1H), 7.18 ~ 7.16 (d, *J* = 8.0

View Article Online
DOI: 10.1039/C3TC30832D

Hz, 1H). ^{13}C NMR (100 MHz, $CDCl_3$) δ (ppm): 149.64, 139.82, 133.33, 132.11, 131.64, 131.43, 130.82, 129.46, 128.38, 128.12, 127.86, 127.45, 126.96, 126.54, 125.93, 125.24, 124.28, 123.69, 123.59, 123.15, 122.77, 122.65, 120.67. MS (APCI): calcd for $C_{27}H_{16}Br_2N_2$: 526.0, found, 527.2 $(M+H)^+$.

2-(3-bromophenyl)-1-(4-bromophenyl)-1H-phenanthro[9,10-d]imidazole (3). Yield: 80%. ^{1}H NMR ($CDCl_3$, 400 MHz) δ (ppm): 8.84 ~8.82 (m, 1H), 8.77 ~ 8.75 (d, *J* = 8.4 Hz, 1H)，8.70 ~ 8.68 (d, *J* = 8.4 Hz, 1H)，7.95 ~ 7.93 (d, *J* = 8.4 Hz, 2H)，7.86 ~ 7.85 (m, 1H)，7.74 ~ 7.72 (m, 1H), 7.68 ~ 7.63 (m, 1H), 7.55 ~ 7.51 (m, 1H), 7.48 ~ 7.45 (m, 1H), 7.34 ~ 7.29 (m, 2H), 7.25 ~ 7.20 (m, 3H), 7.16 ~ 7.12 (m, 1H). ^{13}C NMR (100 MHz, $CDCl_3$) δ (ppm): 149.14, 139.53, 138.14, 137.58, 132.65, 132.16, 132.02, 130.76, 129.72, 129.48, 128.37, 128.05, 127.54, 127.47, 127.00, 126.51, 125.94, 125.29, 124.26, 123.15, 122.76, 122.68, 122.58, 120.73, 95.58. MS (APCI): calcd for $C_{27}H_{16}Br_2N_2$: 526.0, found, 527.1 $(M+H)^+$.

1,2-bis(3-bromophenyl)-1H-phenanthro[9,10-d]imidazole (4). Yield: 75%. ^{1}H NMR ($CDCl_3$, 400 MHz) δ (ppm): 8.85 ~ 8.83 (m, 1H), 8.79 ~ 8.77 (d, *J* = 8.4 Hz, 1H), 8.72 ~ 8.70 (d, *J* = 8.0 Hz, 1H), 7.87 ~ 7.86 (m, 1H), 7.82 ~ 7.79 (m, 1H), 7.77 ~ 7.73 (m, 1H), 7.70 ~ 7.65 (m, 2H), 7.57 ~ 7.47 (m, 4H), 7.36 ~ 7.31 (m, 2H), 7.20 ~ 7.14 (m, 2H). ^{13}C NMR (100 MHz, $CDCl_3$) δ (ppm): 149.12, 139.69, 137.53, 133.34, 132.60, 132.09, 131.39, 129.72, 129.52, 128.39, 128.15, 127.84, 127.54, 127.48, 126.98, 126.55, 125.96, 125.31, 124.28, 123.57, 123.16, 122.78, 122.63, 122.56, 120.73. MS (APCI): calcd for $C_{27}H_{16}Br_2N_2$: 526.0, found, 527.0 $(M+H)^+$.

These target compounds were prepared according to a general procedure described below[27]. A mixture of carbazole (5.0 mmol), the intermediates **1** (**2**, **3** or **4**) (2.0 mmol), CuI (0.2 mmol), 18-crown-6 (0.2 mmol), and K_2CO_3 (20.0 mmol) in 1,3-dimethyltetrahydropyrimidin-2(1H)-one (DMPU) (5.0 ml) was heated at 170 ℃ for 48 h under nitrogen atmosphere. Then cooled to room temperature, the reaction mixture was quenched with 1N HCl, and extracted with dichloromethane, washed with $NH_3{\cdot}H_2O$ and water, and dried by anhydrous $MgSO_4$. The solvent was removed under vacuum, and the residue was purified by column chromatography on silica gel with dichloromethane as eluent. All the target compounds are white powder.

View Article Online
DOI: 10.1039/C3TC30832D

1,2-bis(4-(9H-carbazol-9-yl)phenyl)-1H-phenanthro[9,10-d]imidazole (PhBIDpCP). Yield: 80 %. ^{1}H NMR (400 MHz, $CDCl_3$) δ (ppm): 9.0 (s, 1H), 8.87 ~ 8.84 (d, *J* = 8.4Hz, 1H), 8.78 ~ 8.76 (d, *J* = 8.0Hz, 1H), 8.21 ~ 8.19 (d, *J* = 7.6Hz, 2H), 8.15 ~ 8.13 (d, *J* = 7.6Hz, 2H), 7.97 ~ 7.86 (m, 6H), 7.83 ~ 7.80 (m, 1H), 7.74 ~ 7.72 (m, 1H), 7.65 ~ 7.60 (m, 3H), 7.57 ~ 7.55 (d, *J* = 8.4Hz, 2H), 7.51 ~ 7.35 (m, 10H), 7.32 ~ 7.28 (m, 2H). ^{13}C NMR (100 MHz, $CDCl_3$) δ (ppm): 140.48, 140.43, 131.10, 130.82, 128.64, 128.54, 126.72, 126.64, 126.44, 126.16, 124.46, 123.92, 123.68, 123.24, 120.79, 120.69, 120.41, 120.36, 109.73, 109.38. MS (APCI): calcd for $C_{51}H_{32}N_4$: 700.3, found, 701.2 $(M+H)^+$. Anal. calcd for $C_{51}H_{32}N_4$ (%): C, 87.40; H, 4.60; N, 8.00; Found: C, 87.52; H, 4.74; N, 7.74.

1-(3-(9H-carbazol-9-yl)phenyl)-2-(4-(9H-carbazol-9-yl)phenyl)-1H-phenanthro[9,10-d]imidazole (PhBIDpmCP). Yield: 70%. ^{1}H NMR (400 MHz, $CDCl_3$) δ (ppm): 8.87 ~ 8.85 (d, *J* = 8.4Hz, 1H), 8.77 ~ 8.75 (d, *J* = 8.4Hz, 1H), 8.15 ~ 8.10 (m, 4H), 7.98 (s, 4H), 7.84 ~ 7.81 (m, 3H), 7.75 ~ 7.62 (m, 4H), 7.57 ~ 7.55 (d, *J* = 8.0Hz, 1H), 7.52 ~ 7.30 (m, 11H), 7.28 ~ 7.23 (m, 3H). ^{13}C NMR (100 MHz, $CDCl_3$) δ (ppm): 40.47, 140.36, 139.93, 131.70, 131.13, 129.67, 128.49, 127.84, 127.62, 126.83, 126.61, 126.43, 126.12, 124.47, 123.77, 123.66, 123.21, 120.81, 120.69, 120.59, 120.36, 120.33. MS (APCI): calcd for $C_{51}H_{32}N_4$: 700.3, found, 701.4 $(M+H)^+$. Anal. calcd for $C_{51}H_{32}N_4$ (%): C, 87.40; H, 4.60; N, 8.00; Found: C, 87.53; H, 4.48; N, 7.99.

2-(3-(9H-carbazol-9-yl)phenyl)-1-(4-(9H-carbazol-9-yl)phenyl)-1H-phenanthro[9,10-d]imidazole (PhBIDmpCP). Yield: 72%. ^{1}H NMR (400 MHz, $CDCl_3$) δ (ppm): 8.91 ~ 8.89 (d, *J* = 8.4Hz, 1H), 8.78 ~ 8.76 (d, *J* = 8.4Hz, 1H), 8.71 ~ 8.69 (d, *J* = 8.4Hz, 1H), 8.18 ~ 8.16 (d, *J* = 6.8Hz, 2H), 8.08 ~ 8.06 (d, *J* = 7.6Hz, 2H), 8.01 ~ 7.98 (d, *J* = 8.4Hz, 1H), 7.81 ~ 7.75 (m, 6H), 7.68 ~ 7.64 (m, 2 H), 7.57 ~ 7.52 (m, 2H), 7.40 ~ 7.26 (m, 8H), 7.23 ~ 7.22 (m, 4H), 7.16 ~ 7.14 (m, 2H). ^{13}C NMR (100 MHz, $CDCl_3$) δ (ppm): MS (APCI): 149.75, 140.69, 140.22, 139.38, 137.75, 136.92, 130.62, 130.23, 129.59, 128.86, 128.53, 128.45, 127.95, 127.52, 127.06, 126.52, 126.37, 126.02, 125.97, 125.28, 124.36, 123.87, 123.38, 123.19, 122.83, 120.69, 120.66, 120.51, 120.31, 120.14, 109.51. MS (APCI): calcd for $C_{51}H_{32}N_4$(%): 700.3, found, 701.3 $(M+H)^+$. Anal. calcd for $C_{51}H_{32}N_4$ (%): C, 87.40; H, 4.60; N, 8.00;

View Article Online
DOI: 10.1039/C3TC30832D

Found: C, 87.50; H, 4.46; N, 8.04.

1,2-bis(3-(9H-carbazol-9-yl)phenyl)-1H-phenanthro[9,10-d]imidazole (PhBIDmCP). Yield: 50%. ^{1}H NMR (400 MHz, $CDCl_3$) δ (ppm): *8.88 ~ 8.86* (d, *J* = 8.0Hz, 1H), 8.82 ~ 8.80 (d, *J* = 8.0Hz, 1H), 8.72 ~ 8.70 ((d, *J* = 8.4Hz, 1H), 8.14 ~ 8.12 (d, *J* = 7.6Hz, 2H), 8.06 ~ 7.99 (m, 3H), 7.92 ~ 7.88(m, 2H), 7.76 ~ 7.58 (m, 8H), 7.48 ~ 7.39 (m, 2H), 7.32 ~ 7.14 (m, 10H), 7.00 (s, 2H). ^{13}C NMR (100 MHz, $CDCl_3$) δ (ppm): 149.66, 140.77, 140.28, 139.99, 137.84, 131.84, 130.40, 129.63, 129.14, 128.45, 128.41, 128.17, 128.00, 127.69, 127.60, 127.51, 126.50, 126.29, 126.02, 125.37, 124.42, 123.67, 123.41, 123.16, 122.83, 122.78, 120.78, 120.53, 120.41, 120.32, 120.14, 109.69, 109.17. MS (APCI): calcd for $C_{51}H_{32}N_4$: 700.3, found, 701.3 $(M+H)^+$. Anal. calcd for $C_{51}H_{32}N_4$ (%): C, 87.40; H, 4.60; N, 8.00; Found: C, 87.34; H, 4.52; N, 8.14.

3. Results and Discussion

3.1. Synthesis

As shown in Scheme 1, the PhBI-Br_2 intermediates (the compounds 1, 2, 3 and 4) were synthesized in one-pot reactions in high yields (> 75 %) (See the Experimental Section). The target products were prepared through the typical Ullmann coupling reaction of carbazole and PhBI-Br_2 intermediates, and the crude products were purified by column chromatography on silica gel using dichloromethane as the eluent. The simple synthetic method provides a common and facile way to construct phenanthroimidazole derivatives with tunable photoelectronic properties through judicious engineering of the linkage modes. Repeated temperature-gradient vacuum sublimation is required for further purification of these materials used in OLEDs. All the target products were fully characterized by ^{1}H NMR, ^{13}C NMR, mass spectrometry and elemental analysis.

View Article Online
DOI: 10.1039/C3TC30832D

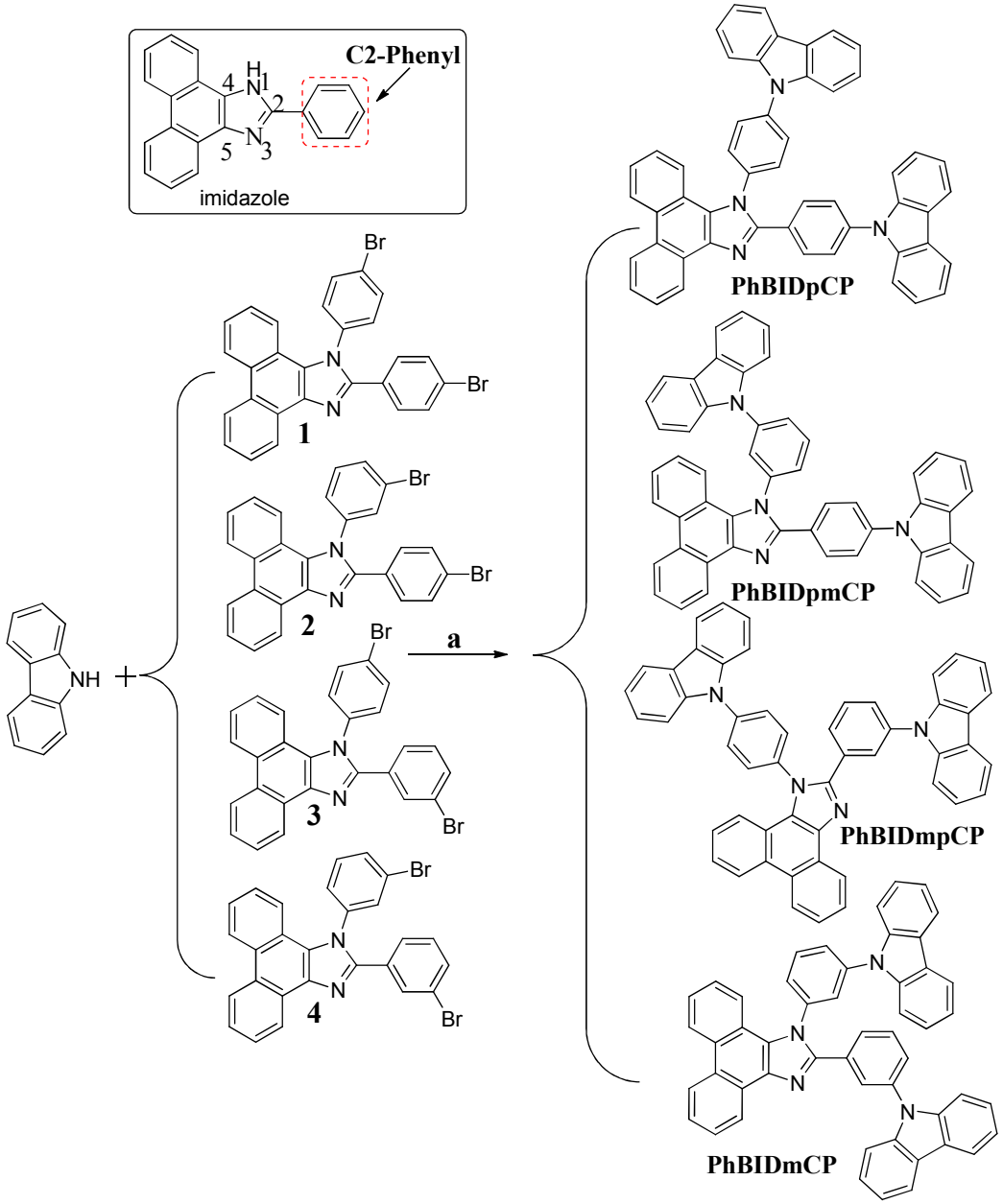

Scheme 1 The synthetic routes of PhBIDpCP, PhBIDpmCP, PhBIDmpCP and PhBIDmCP. Reagents and conditions: (a) CuI, K_2CO_3, 18-Crown-6, 180 ℃, 48 h.

3.2. Thermal properties

All the phenanthroimidazole and carbazole hybrids show high thermal stabilities (Fig. 1). The thermal-decomposition temperatures (T_d) for 5 % weight loss are in range of 468 ~ 514 ℃. In particular, their glass-transition temperatures (T_g) are ranging from 147 to 282 ℃, which are distinctly higher than that of carbazole based

View Article Online
DOI: 10.1039/C3TC30832D

analogous, such as CBP (62 ℃) and mCP (60 ℃)[17], pPhBINCP(113℃) and mPhBINCP(113℃)[22]. The significant enhancement of Tg can be attributed to the introduction of two carbazole units to phenanthroimidazole moiety, which would reduce the possibility of phase separation upon heating, and prolong the lifetime of the devices. Specifically, the compound PhBIDpCP with carbazole at *para*- positions of the C2-phenyl and N1-phenyl of the phenanthroimidazole shows the highest T_g reached to 282 ℃, which further verified the principle that the small energetic disorder the *para*- positions of the C2-phenyl of the phenanthroimidazole can efficiently enhance the morphological stability[28]. It is regret that no obvious glass transition temperatures (T_g) are observed for the compound PhBIDpmCP.

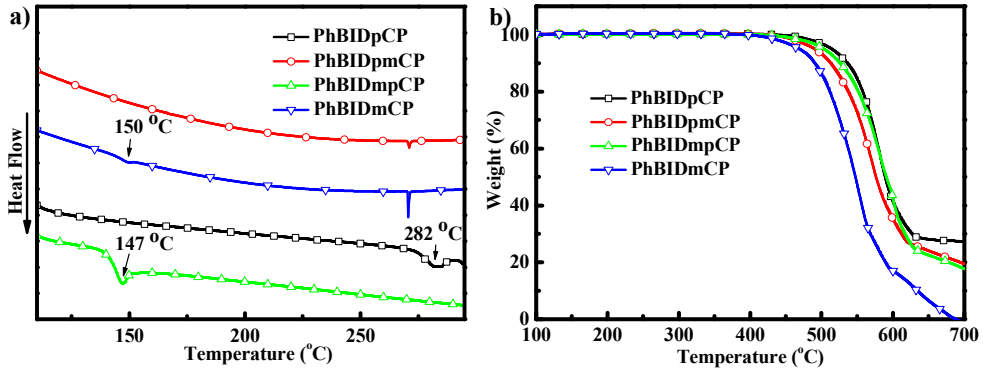

Fig. 1 DSC (a) and TGA (b) Curves of PhBIDpCP, PhBIDpmCP, PhBIDmpCP and PhBIDmCP.

3.3. Morphology properties

Since the excellent film-forming properties of light emitting materials are crucial for the high performances of the devices, the surface morphologies of vacuum-deposited thin films of four new compounds, PhBIDmpCP, PhBIDmCP, PhBIDpCP and PhBIDpmCP were studied by atomic force microscopy (AFM). As shown in Fig. 2, the organic films exhibit a root-mean-square (RMS) roughness of 0.358, 0.445, 0.443 and 0.457 nm for PhBIDmpCP, PhBIDmCP, PhBIDpCP and PhBIDpmCP, respectively. The relatively small RMS of the thin films for these hosts make them desirable for the high-vacuum deposition process. Specifically, the thin film of PhBIDmpCP shows the lowest RMS, which meets the necessity for high efficiency device.

View Article Online
DOI: 10.1039/C3TC30832D

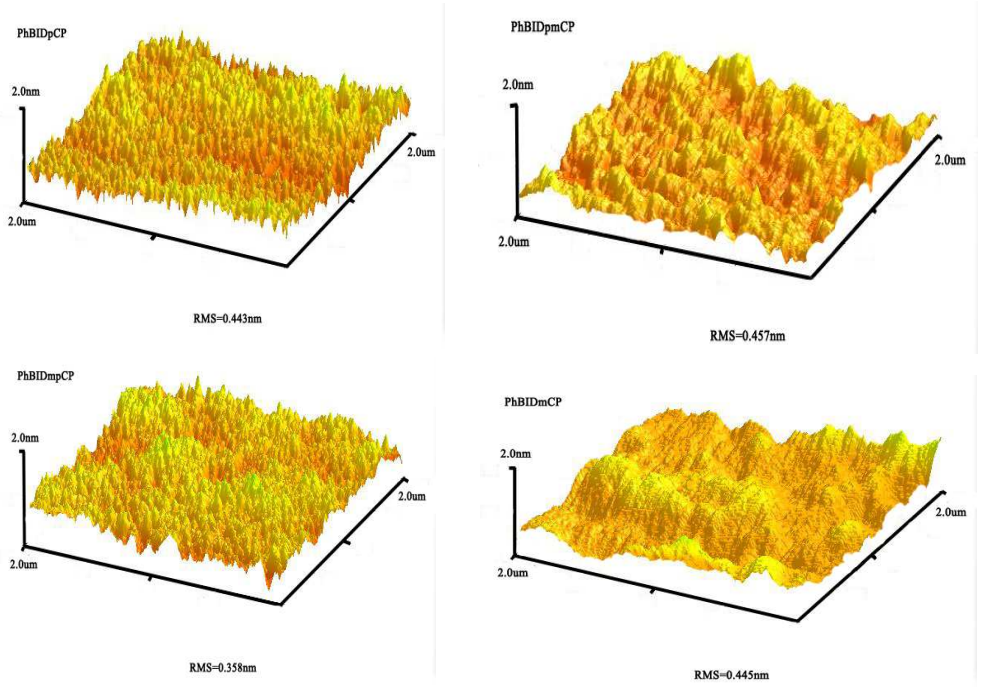

Fig. 2 The AFM topographic images of PhBIDpCP, PhBIDpmCP, PhBIDmpCP and PhBIDmCP.

3.4. Photophysical properties

The absorption and fluorescence spectra of these compounds in CH_2Cl_2 solution and film state were studied to investigate the relationship between linkage modes and the photophysical properties (Fig. 3). For the four target compounds, their absorption spectra exhibit no distinct differences and all exhibit two peaks at around 290 nm and 336 nm in CH_2Cl_2 solution. The absorption peaks at about 290 nm for the four compounds could be assigned to the carbazole centered n-π* transition, while the absorption bands between 330 to 340 nm arise from the π-π* transition from the carbazole and the phenanthroimidazole moiety. The photoluminescence spectra for PhBIDpCP and PhBIDpmCP show a sharp emission peak at 383 nm and a shoulder peak at 403 nm, while for PhBIDmpCP and PhBIDmCP, two peaks blue shift to 368 nm and 488 nm due to their limited conjugation of the *meta* linkage to C2-phenyl compared with *para* linked former two compounds. Above all, the absorption and emission spectra of these compounds varied with the linkage positions of the carbazole to phenanthroimidazole, the compounds with the same substituted position (*para* or *meta)* to C2-phenyl almost display the similar spectrum. The absorbance and

View Article Online
DOI: 10.1039/C3TC30832D

photoluminescence of the four compounds in film state exhibit a similar red shift phenomenon compared with that in the solution. The shoulder emission peaks has been weakened because the intramolecular energy transfer could be effectively blocked in the solid state.

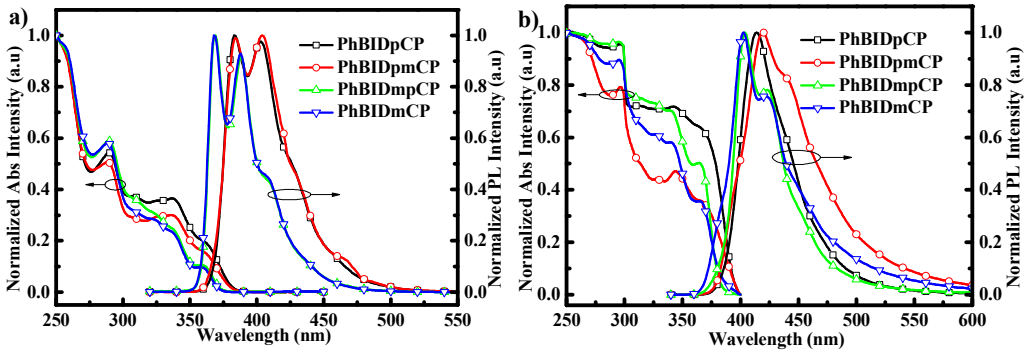

Fig. 3 (a) UV-visible absorption and PL spectra of PhBIDpCP, PhBIDpmCP, PhBIDmpCP and PhBIDmCP in dilute CH_2Cl_2 solution; (b) PL spectra of PhBIDpCP, PhBIDpmCP, PhBIDmpCP and PhBIDmCP in film state.

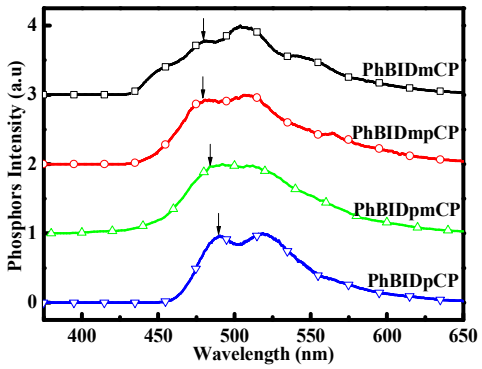

Fig. 4 Phosphorescence spectra of PhBIDpCP, PhBIDpmCP, PhBIDmpCP and PhBIDmCP in 2-methyltetrahydrofuran at 77 K.

The triplet energies (E_T) of these new compounds have also been determined by the highest energy vibronic sub-band of the phosphorescence spectra at 77 K (Fig. 4). They all show low E_T (2.54 for PhBIDpCP, 2.56 eV for PhBIDpmCP, 2.59 eV for PhBIDmpCP and 2.58 eV for PhBIDmCP). The relative lower E_T of PhBIDpCP can be ascribed to the two *para*-conjugations between the carbazole and phenanthroimidazole moieties. The E_T values of the four compounds are all higher than that of $Ir(ppy)_3$ (2.40 eV), implying that they may act as appropriate host materials for green phosphorescent emitters.

3.5. Electrochemical properties

View Article Online
DOI: 10.1039/C3TC30832D

The electrochemical properties of the four compounds were studied in solution through cyclic voltammetry (CV) measurements using $Ag/AgNO_3$ as the reference electrode. The cyclic voltammograms are shown in Fig. 5 and the electrochemical data are summarized in Table 1. All the compounds exhibit similar reversible oxidation waves as most carbazole derivatives[29]. The highest occupied molecular orbital (HOMO) energy levels of the compounds were determined from the onset of the oxidation potentials with regard to energy level of Ag/Ag^+ (4.6 eV below vacuum). The lowest unoccupied molecular orbital (LUMO) energy levels of the compounds were calculated from the HOMO energy levels and energy gap deduced from their absorption spectra. The HOMO levels of the four compounds vary in range of -5.82 ~ -5.87 eV and the LUMO levels range from -2.49 to -2.62 eV (Table 1), depending on the linkage modes of the electronic donor and acceptor moieties.

Table 1 The photophysical, electrochemistry and thermal data of phenanthroimidazole derivatives

Compound	$\lambda_{max,abs}$ (nm)		λ_{em} (nm)		E_g	HOMO/LUMO	HOMO/LUMO	E_T	T_g/T_d
	Solution[a]	Film[b]	Solution[a]	Film[b]	(eV)	MO (eV)[c]	MO (eV)[d]	(eV)[e]	(℃)
PhBIDpCP	338/289	342/296	403/383	414	3.25	-5.87/-2.62	-5.33/-2.33	2.54	282/514
PhBIDpmCP	338/289	344/297	404/384	419	3.27	-5.84/-2.57	-5.35/-2.30	2.56	---/490
PhBIDmpCP	336/290	340/295	388/368	422/403	3.32	-5.82/-2.50	-5.36/-2.29	2.59	147/503
PhBIDmCP	335/289	340/295	388/368	421/403	3.34	-5.83/-2.49	-5.38/-2.27	2.58	150/468

[a] Measured in CH_2Cl_2 solvent at room temperature. [b] Measured in solid state. [c] Determined from the onset of the oxidation. [d] Values from DFT calculation. [e] Measured in 2-methyltetrahydrofuran at 77 K.

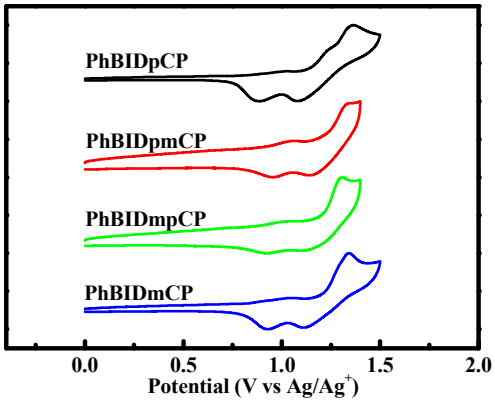

Fig. 5 Cyclic voltammgrams of PhBIDpCP, PhBIDpmCP, PhBIDmpCP and PhBIDmCP.

3.6. Theoretical calculations

PhBIDpCP **PhBIDpmCP** **PhBIDmpCP** **PhBIDmCP**

View Article Online
DOI: 10.1039/C3TC30832D

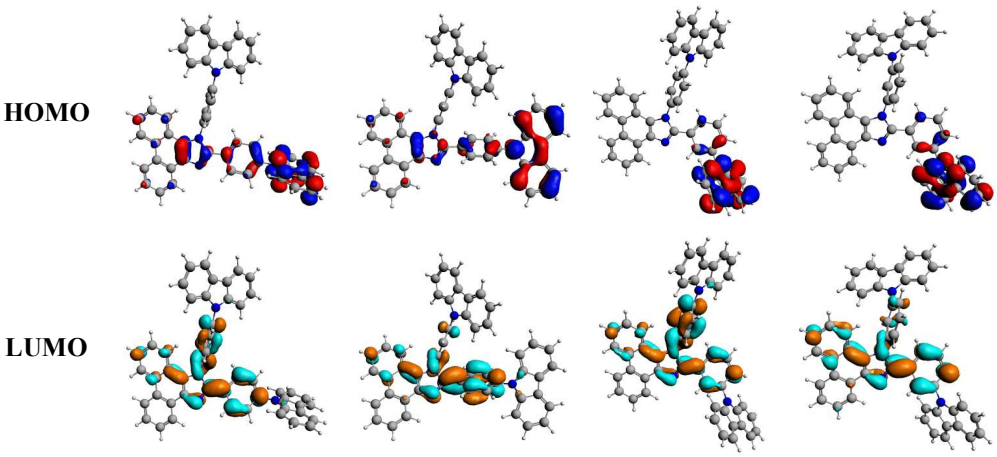

Fig. 6 Calculated spatial distributions of the HOMO and LUMO energy densities of the phenanthroimidazole derivatives.

A quantum chemical calculations was performed on the phenanthroimidazole derivatives at the B3LYP/6-31G(d) theoretical level. As depicted in Fig. 6. The electron density distributions of the HOMO and LUMO of the phenanthroimidazole derivatives are localized predominantly on the electron-rich carbazole and electron-deficient phenanthroimidazole fragments, respectively. The difference among the four compounds could be attributed to the linkage modes of carbazole to the C2-phenyl of the phenanthroimidazole. With the carbazole moiety conjugated to the *meta* of the C2-phenyl, the distributions of the HOMO and LUMO are completely separated, which are consistent with the aim of structure engineering that the p type unit is responsible for hole transporting and the n type group plays a key role in electron transporting. The separation between the HOMO and LUMO orbitals is beneficial to the efficient charge-carrier transport and the prevention of reverse energy transfer. The values of the calculation HOMO and LUMO levels are listed in Table 1.

3.7. Bipolar transporting characteristics

To investigate the bipolar transporting properties of these compounds, the hole only device: ITO/NPB(10 nm)/host(30 nm)/NPB(10 nm)/Al(100 nm) and the electro-only device: ITO/BCP(10 nm)/host(30 nm)/BCP(30 nm)/LiF(1 nm)/Al(100 nm) were fabricated. 1,4-bis[(1-naphthylphenyl)amino]biphenyl (NPB) and 2,9-dimethyl-4,7-diphenyl-1,10-phenanthroline (BCP) layers were used to prevent

View Article Online
DOI: 10.1039/C3TC30832D

electron and hole injection from the cathode and anode, respectively[14]. The current density versus voltage curves of the devices were shown in Fig. 7. Generally, the hole mobility are much higher (about 1000 times) than the electron mobility in organic semiconducting materials[30]. For the hosts PhBIDpCP, PhBIDpmCP and PhBIDmCP, the hole only devices show higher current density than the electron only devices at the same voltage. Interestingly, for compounds PhBIDmpCP, the electron only device shows higher current density than the hole only device at the same voltage. It may be attributed to the difference of molecular packing and nanostructures of PhBIDpCP, PhBIDpmCP, PhBIDmpCP and PhBIDmCP in thin film systems. The charge densities of hole only and electron only devices are often dependent on the interfacial characteristics and mobility of host material. As for the interfacial effect, we can only provide a little rational explanation from the AFM (RMS: PhBIDmpCP < PhBIDmCP ≈ PhBIDpCP < PhBIDpmCP, see Fig 2).

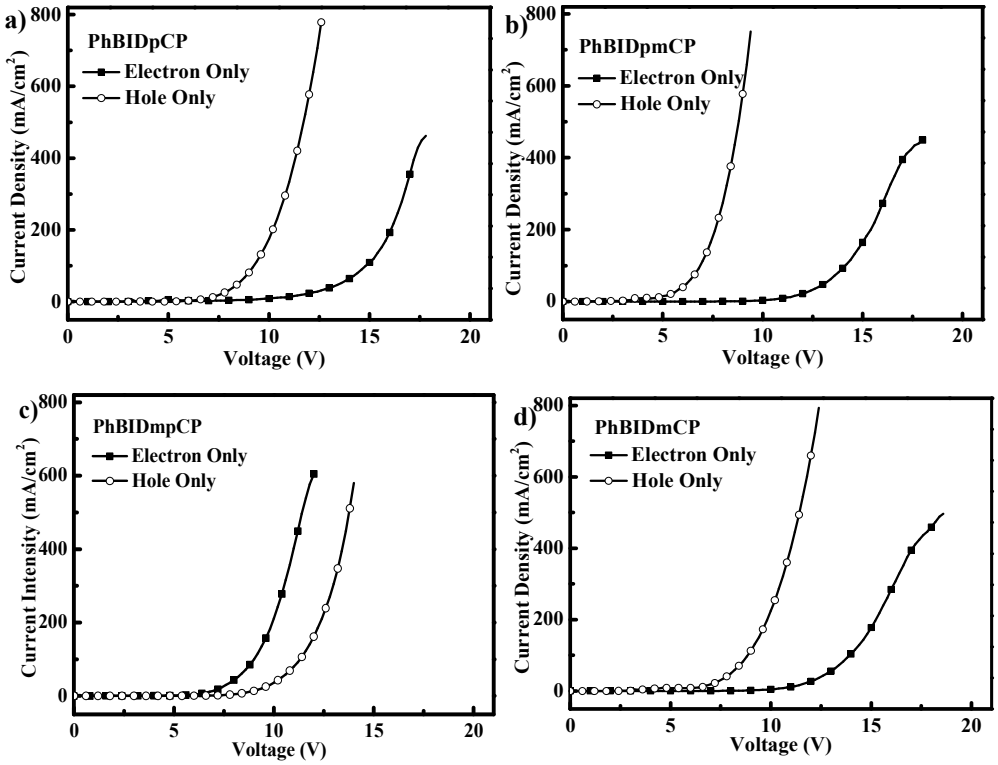

Fig. 7 Current density versus voltage characteristics of the hole-only and electron-only devices for PhBIDpCP, PhBIDpmCP, PhBIDmpCP and PhBIDmCP.

In order to further explain this interesting phenomenon, we selected PhBIDpCP,

View Article Online
DOI: 10.1039/C3TC30832D

PhBIDmpCP as representative and tested their electron and hole mobility using the conventional time of flight (TOF) technique based on the device configuration of [ITO/ PhBIDpCP or PhBIDmpCP (um)/Al]. Fig. 8 shows typical TOF transients of holes/electron for complex PhBIDpCP and PhBIDmpCP under an applied field. For the compounds PhBIDmpCP, the electron mobility (3.92* 10^{-4} cm^2/Vs) is larger than the hole mobility (3.27* 10^{-4} cm^2/Vs), while it is reversed for the compounds PhBIDpCP, with the electron mobility (2.36* 10^{-4} cm^2/Vs) *vs* the hole mobility (3.14* 10^{-4} cm^2/Vs). The results further explain why the electron only device based on PhBIDmpCP has the highest electron density among these new hosts. It is also demonstrate that the charge transport of organic semiconductors is strongly molecular packing and morphology dependent and organic molecules with similar molecular structures can exhibit remarkably different mobility[31]. For the two representative compounds, both the hole and electron mobility is at the level of 10^{-4} cm^2/V s, which further demonstrate their bipolar properties as host materials.

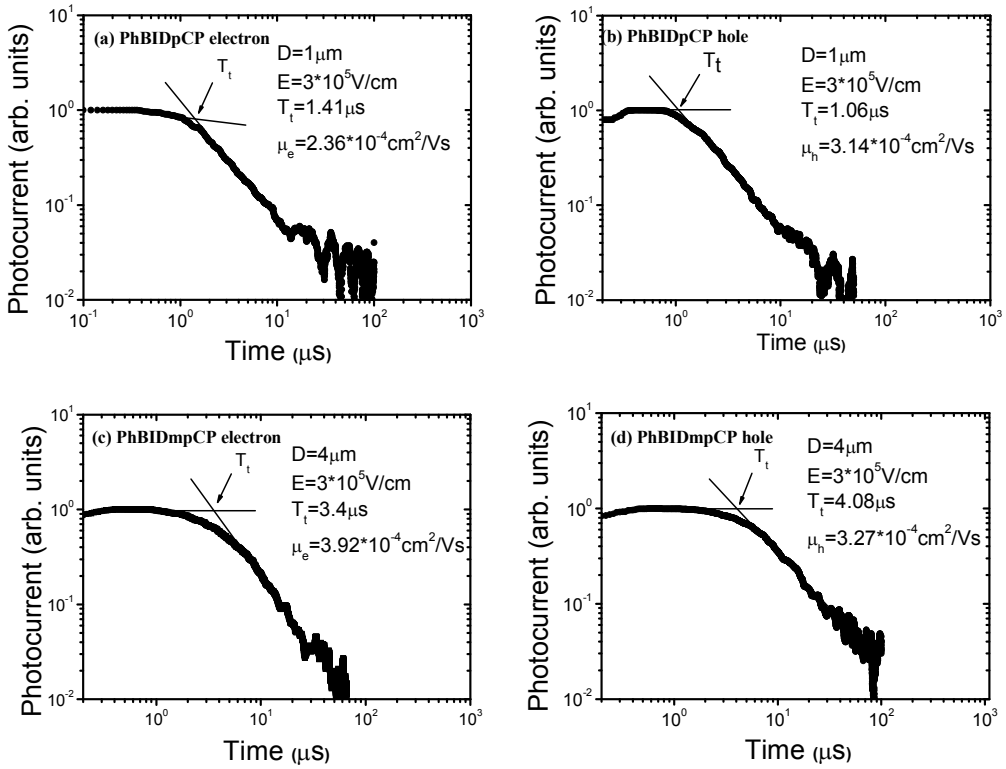

Fig. 8 Log of the photocurrent vs. the log of time in a time-of-flight measurement. The electron

View Article Online
DOI: 10.1039/C3TC30832D

mobility (μ) was calculated from the values of the transit time (T_t), the sample thickness and the applied voltage (V) according to the equation $\mu = D^2/(VT_t)$

3.8. Electrophosphorescent OLED Characterization

To evaluate the suitability of these bipolar phenanthroimidazole derivatives as host material in green phosphorescent OLEDs, devices with the configuration of ITO/MoO_3(10 nm)/NPB(80 nm)/TCTA(5 nm)/Host: 9wt% $Ir(ppy)_3$(20 nm)/TmPyPB (45 nm)/LiF(1 nm)/Al(100 nm) (Host: PhBIDpCP for Device A; PhBIDpmCP for Device B; PhBIDmpCP for Device C; PhBIDmCP for Device D) were fabricated. NPB acts as the hole-transporting layer and TCTA is the exciton blocking layer. $Ir(ppy)_3$ doped into these hosts was used as the emitting layer, and the best electroluminescence (EL) performance was achieved with 9 wt % $Ir(ppy)_3$ for all the hosts. TmPyPB serves as both the electron-transporting layer and hole-blocking layer. MoO_3 and LiF (lithium fluoride) serves as the hole- and electron-injecting layers, respectively. The energy level diagram of the devices based on the phenanthroimidazole derivatives is shown in Fig. 9.

As shown in Fig. 10, all the fabricated devices emit brightly green light with the CIE coordinates of (0.30, 0.63) when the bias is applied to the anode/cathode. The EL spectra of the devices are almost the same as the emission spectrum of the $Ir(ppy)_3$, which indicates that the EL is indeed derived from the phosphorescent emitter and the triplet energy transfer from the host to the dopant is completely. The results demonstrate in turn that the triplet energies of the host materials are high enough to the phosphorescent emitter $Ir(ppy)_3$.

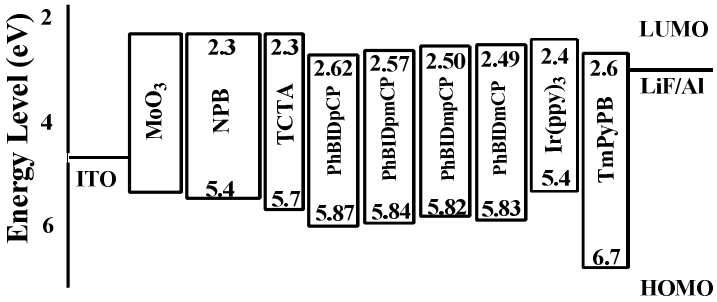

Fig. 9 Energy level diagram of the devices based on the phenanthroimidazole derivatives.

View Article Online
DOI: 10.1039/C3TC30832D

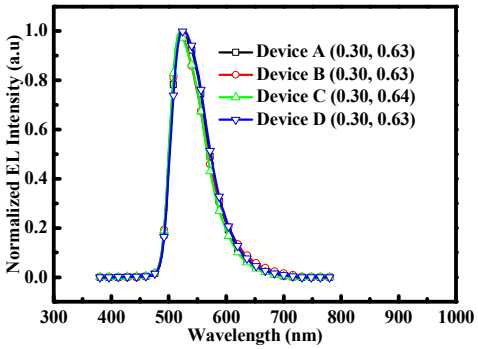

Fig. 10 EL spectra of the devices based on the phenanthroimidazole derivatives.

Fig. 11 shows the *J-V-L* characteristic, efficiency-versus-current density curves of the four devices, and the key device performance parameters are summarized in Table 2. The devices A-D display low turn-on voltages in a range of 2.8 ~ 3.0 V, which is attributed to the bipolar transporting capabilities and the suitable HOMO and LUMO energy levels of these hosts used. As shown in Fig. 9, there are injection barriers of approximately 0.2-0.3 eV for electrons at TCTA/EML interface and about 0.9 eV for the hole at EML/TmPyPB interfaces, which implies that the carriers can be confined the EML layer and resulted in high exciton formation efficiencies even under high current densities. Definitely, all the devices exhibit high and stable efficiencies.

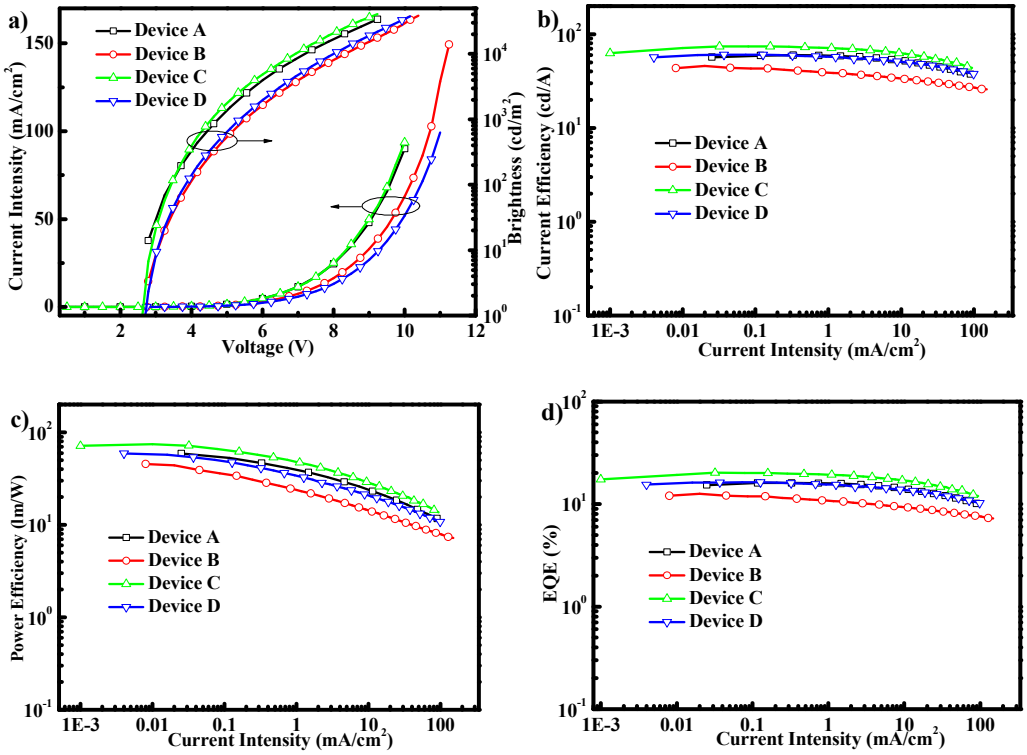

View Article Online
DOI: 10.1039/C3TC30832D

Fig. 11 (a) Current density-voltage-luminance characteristics (*J-V-L*) of device A-D; (b) Current efficiency versus current density curves for device A-D; (c) Power efficiency versus current density curves for device A-D; (d) External quantum efficiency versus current density for device A-D.

Device C with the PhBIDmpCP as the host achieves the best EL performance, with a maximum current and power efficiency of 74.3 cd/A and 74.4 lm/W, respectively, corresponding maximum EQE of 20.2 %. Devices A, B and D exhibit a maximum current efficiency of 59.6 cd/A, 45.7 cd/A, 60.3 cd/A and power efficiencies of 59.4 lm/W, 45.6 lm/W, 59.2 lm/W, respectively. Definitely, all of these values are higher than those of the CBP-hosted device[16]. It is worth noting that both the current and power efficiencies of the Device A-D are in the order of C > D ≈ A > B. The result can be explained by the current density differences at the same voltage of the electron- and hole- only devices of these hosts, which in turn demonstrates that the electron injection from cathode into hosts are in the order of PhBIDmpCP > PhBIDmCP ≈ PhBIDpCP > PhBIDpmCP. Meanwhile, because of the excellent electron/hole mobility of PhBIDmpCP, device C exhibits low efficiency roll-off at high luminance, and the external quantum efficiency (EQE) is still up to 20.0% and 19.3% at the luminance of 100 cd/m^2 and 1000 cd/m^2, respectively. Notably, when the luminance reaches as high as 10000 cd/m^2, the EQE only slightly rolls down to 16.1%. On the other side, the completely separation between the HOMO and LUMO levels in these host materials, is also beneficial for efficient charge transport.

Table 2 EL performances of devices A-D based on the phenanthroimidazole derivatives

Device	host	V_{on}[a] (V)	L_{max}[b] (cd/m^2)	Voltage for L_{max}(V)	$\eta_{c,max}$[c] (cd/A)	$\eta_{p,max}$[d] (lm/W)	EQE_{max} (%)	CIE(x, y)[e]
A	**PhBIDpCP**	2.8	33670	10.0	59.6	59.4	16.1	(0.30, 0.63)
B	**PhBIDpmCP**	3.0	38500	11.2	45.7	45.6	12.6	(0.30, 0.63)
C	**PhBIDmpCP**	2.8	40890	10.0	74.3	74.4	20.2	(0.30, 0.64)
D	**PhBIDmCP**	3.0	37520	11.0	60.3	59.2	16.3	(0.30, 0.63)

[a] The turn-on voltage (L = 1 cd/m^2). [b] Maximum luminance. [c] Maximum current efficiency. [d] Maximum power efficiency. [e] The brightness is 100 cd/m^2.

4. Conclusions

In summary, a series of simple phenanthroimidazole/carbazoles(1:2) hybrids as

View Article Online
DOI: 10.1039/C3TC30832D

bipolar host materials have been developed by using different linkage modes. The photophysical, charge transport abilities, film morphology and electrochemical properties of these compounds can be controllably tuned by the different linkage modes between the phenanthroimidazole and the two carbazoles, and further to affect the device performances. The introduction of two carbazole group to phenanthroimidazole moiety can significally improve the thermal stability of the host materials. Device with 9 wt % $Ir(ppy)_3$ hosted with PhBIDmpCP achieves a maximum external quantum efficiency as high as 20.2% and exhibits an efficiency roll-off at high luminance. This work definitely demonstrates that tradeoffs among the bipolar property, the triplet energy, charge transport abilities and the energy levels can be controlled through judicious tuning the linkage modes between the electron donor and acceptor.

Acknowledgements

This research work was supported by the NSFC/China (21161160442, 51203056) , the National Basic Research Program of China (973 Program 2013CB922104), Wuhan Science and Technology Bureau (NO: 01010621227) and the Open Research Fund of State Key Laboratory of Polymer Physics and Chemistry.

References

1. B. W. D'Andrade and S. R. Forrest, *Adv. Mater.*, 2004, **16**, 1585.
2. T. Zhang, Y. Liang, J. Cheng and J. Li, *J. Mater. Chem. C.*, 2013, **1**, 757.
3. C. J. Zheng, J. Ye, M.-F. Lo, M.-K. Fung, X. M. Ou, X. H. Zhang and C. S. Lee, *Chem. Mater.*, 2012, **24**, 643.
4. M. S. Lin, L. C. Chi, H. W. Chang, Y. H. Huang, K. C. Tien, C. C. Chen, C. H. Chang, C. C. Wu, A. Chaskar, S. H. Chou, H. C. Ting, K. T. Wong, Y. H. Liu and Y. Chi, *J. Mater. Chem.*, 2012, **22**, 870.
5. J. Chen, C. Shi, Q. Fu, F. Zhao, Y. Hu, Y. Feng and D. Ma, *J. Mater. Chem.*, 2012, **22**, 5164.
6. M. A. Baldo, C. Adachi and S. R. Forrest, *Phys. Rev. B.*, 2000, **62**, 10967.

View Article Online
DOI: 10.1039/C3TC30832D

7. R. J. Holmes, S. R. Forrest, Y. J. Tung, R. C. Kwong, J. J. Brown, S. Garon and M. E. Thompson, *Appl. Phys. Lett.*, 2003, **82**, 2422.
8. J. He, H. Liu, Y. Dai, X. Ou, J. Wang, S. Tao, X. Zhang, P. Wang and D. Ma, *J. Phys. Chem. C.*, 2009, **113**, 6761.
9. W. S. Jeon, T. J. Park, S. Y. Kim, R. Pode, J. Jang and J. H. Kwon, *Appl. Phys. Lett.*, 2008, **93**, 063303.
10. M. S. Park and J. Y. Lee, *Org. Electron.*, 2013, **14**, 1291.
11. S. H. Cheng, S. H. Chou, W. Y. Hung, H. W. You, Y. M. Chen, A. Chaskar, Y.-H. Liu and K. T. Wong, *Org. Electron.*, 2013, **14**, 1086.
12. W. Y. Hung, G. M. Tu, S. W. Chen and Y. Chi, *J. Mater. Chem.*, 2012, **22**, 5410.
13. C. H. Chang, M. C. Kuo, W. C. Lin, Y. T. Chen, K. T. Wong, S. H. Chou, E. Mondal, R. C. Kwong, S. Xia, T. Nakagawa and C. Adachi, *J. Mater. Chem.*, 2012, **22**, 3832.
14. H. H. Chou and C. H. Cheng, *Adv. Mater.*, 2010, **22**, 2468.
15. Z. Q. Gao, M. Luo, X. H. Sun, H. L. Tam, M. S. Wong, B. X. Mi, P. F. Xia, K. W. Cheah and C. H. Chen, *Adv. Mater.*, 2009, **21**, 688.
16. Y. Tao, Q. Wang, C. Yang, Q. Wang, Z. Zhang, T. Zou, J. Qin and D. Ma, *Angew. Chem. Int. Ed.,* 2008, **47**, 8104.
17. M. H. Tsai, Y. H. Hong, C. H. Chang, H. C. Su, C. C. Wu, A. Matoliukstyte, J. Simokaitiene, S. Grigalevicius, J. V. Grazulevicius and C. P. Hsu, *Adv. Mater.*, 2007, **19**, 862.
18. Y. Yuan, D. Li, X. Zhang, X. Zhao, Y. Liu, J. Zhang and Y. Wang, *New. J. Chem.*, 2011, **35**, 1534.
19. Y. Zhang, S. L. Lai, Q. X. Tong, M. F. Lo, T. W. Ng, M. Y. Chan, Z. C. Wen, J. He, K. S. Jeff, X. L. Tang, W. M. Liu, C. C. Ko, P. F. Wang and C. S. Lee, *Chem. Mater.*, 2011, **24**, 61.
20. Z. Wang, P. Lu, S. Chen, Z. Gao, F. Shen, W. Zhang, Y. Xu, H. S. Kwok and Y. Ma, *J. Mater. Chem.*, 2011, **21**, 5451.
21. Y. Zhang, S. L. Lai, Q. X. Tong, M. Y. Chan, T. W. Ng, Z. C. Wen, G. Q. Zhang, S. T. Lee, H. L. Kwong and C. S. Lee, *J. Mater. Chem.*, 2011, **21**, 8206.
22. H. Huang, Y. Wang, S. Zhuang, X. Yang, L. Wang and C. Yang, *J. Phys. Chem. C.*, 2012, **116**, 19458.
23. C. Lee, W. Yang and R. G. Parr, *Phys. Rev. B.*, 1988, **37**, 785.

View Article Online
DOI: 10.1039/C3TC30832D

24. A. D. Boese and N. C. Handy, *J. Chem. Phys.*, 2002, **116**, 9559.

25. S. R. Forrest, D. D. C. Bradley and M. E. Thompson, *Adv. Mater.*, 2003, **15**, 1043.

26. F. C. Krebs and H. Spanggaard, *J. Org. Chem.*, 2002, **67**, 7185.

27. S. Gong, Y. Zhao, C. Yang, C. Zhong, J. Qin and D. Ma, *J. Phys. Chem. C.*, 2010, **114**, 5193.

28. Y. Shirota, *J. Mater. Chem.*, 2000, **10**, 1.

29. G. Zotti, G. Schiavon, S. Zecchin, J.-F. Morin and M. Leclerc, *Macromolecules.*, 2002, **35**, 2122.

30. H. Antoniadis, M. A. Abkowitz and B. R. Hsieh, *Appl. Phys. Lett.*, 1994, **65**, 2030.

31. Y. Yuan, D. Li, X. Q. Zhang, X. J. Zhao, Y. Liu, J. Y. Zhang and Y. Wang *New.J. Chem.,* 2011, **35**, 1534.